Joule

CellPress

Article

Low-Symmetry Rhombohedral GeTe Thermoelectrics

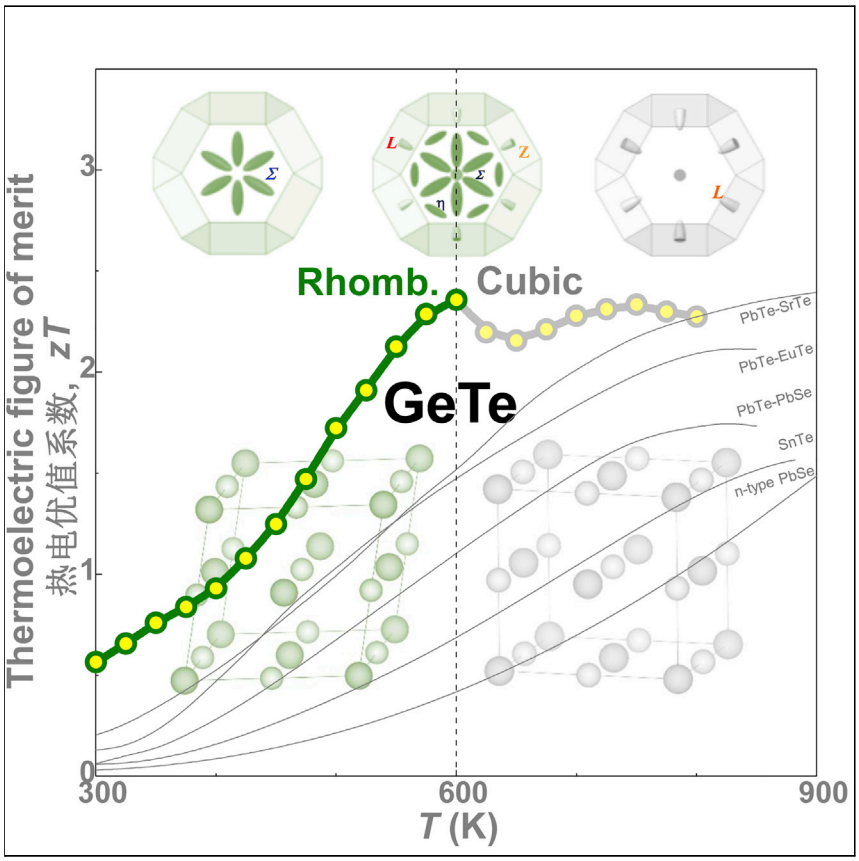

Cubic GeTe thermoelectrics have been historically focused on, while this work utilizes a slight symmetry-breaking strategy to converge the split valence bands, to reduce the lattice thermal conductivity and therefore realize a record thermoelectric performance, all enabled in GeTe in a rhombohedral structure. This not only promotes GeTe alloys as excellent materials for thermoelectric power generation below 800 K, but also expands low-symmetry materials as efficient thermoelectrics.

Juan Li, Xinyue Zhang, Zhiwei Chen, ..., Lidong Chen, G. Jeffrey Snyder, Yanzhong Pei

yanzhong@tongji.edu.cn

HIGHLIGHTS

Rhombohedral GeTe shows a record thermoelectric figure of merit ($zT \sim 2.4$)

This is enabled by the slight reduction of symmetry from its cubic analogs

The symmetry breaking splits bands but enables an overall band convergence

The principle expands low-symmetry materials as efficient thermoelectrics

Li et al., Joule 2, 976–987
May 16, 2018
https://doi.org/10.1016/j.joule.2018.02.016

Joule

CellPress

Article

Low-Symmetry Rhombohedral GeTe Thermoelectrics

Juan Li,[1,6] Xinyue Zhang,[1,6] Zhiwei Chen,[1] Siqi Lin,[1] Wen Li,[1] Jiahong Shen,[2] Ian T. Witting,[4] Alireza Faghaninia,[5] Yue Chen,[2] Anubhav Jain,[5] Lidong Chen,[3] G. Jeffrey Snyder,[4] and Yanzhong Pei[1,7,*]

SUMMARY

High-symmetry thermoelectric materials usually have the advantage of very high band degeneracy, while low-symmetry thermoelectrics have the advantage of very low lattice thermal conductivity. If the symmetry breaking of band degeneracy is small, both effects may be realized simultaneously. Here we demonstrate this principle in rhombohedral GeTe alloys, having a slightly reduced symmetry from its cubic structure, to realize a record figure of merit ($zT \sim 2.4$) at 600 K. This is enabled by the control of rhombohedral distortion in crystal structure for engineering the split low-symmetry bands to be converged and the resultant compositional complexity for simultaneously reducing the lattice thermal conductivity. Device ZT as high as 1.3 in the rhombohedral phase and 1.5 over the entire working temperature range of GeTe alloys make this material the most efficient thermoelectric to date. This work paves the way for exploring low-symmetry materials as efficient thermoelectrics.

INTRODUCTION

Owing to the growing demand for clean and sustainable energy, thermoelectric (TE) conversion that directly converts waste heat to electricity[1] has attracted increasing attention. However, the expanded application of thermoelectric technology is hindered by its relatively low energy conversion efficiency. The foremost challenge in developing these materials is the improvement of the thermoelectric figure of merit, which is evaluated by $zT = S^2T/\rho(\kappa_E + \kappa_L)$, where S, T, ρ, κ_E, and κ_L are Seebeck coefficient, absolute temperature, electrical resistivity, and electronic and lattice components of the thermal conductivity, respectively.

Since S, ρ, and κ_E are strongly linked with each other, decoupling these parameters by the involvement of many conducting band valleys[2–4] is known to be particularly successful. This is because possessing many degenerate band valleys, (N_v), enables a low resistivity through multiple conducting channels while still maintaining a high Seebeck coefficient. The mobility is normally unaffected by N_v, but there may be some reduction due to intervalley scattering. High valley degeneracy occurs most frequently at a low-symmetry point in the reciprocal space of a high-symmetry structure, due to the presence of many equivalent symmetry operations. This aspect has enabled the majority of thermoelectric advancements achieved in cubic materials including Si-Ge,[5] (Pb,Sn)Te,[2,6,7] Mg_2Si,[8] $CoSb_3$,[9] $Cu_2(Se, S)$,[10] $AgSbTe_2$,[11] La_3Te_4,[12] clathrates,[13] half-Heuslers[14] and rhombohedral Bi_2Te_3,[15,16] all of which have a large valley degeneracy due to band symmetry[3] and many times also band convergence.[2] Indeed, an attempt at tuning a chalcopyrite structure to a

Context & Scale

Thermoelectric materials enable a heat flow to be directly converted to a flow of charge carriers for generating electricity. The crystal structure symmetry is one of the most fundamental parameters determining the properties of a crystalline material including thermoelectrics. The common belief currently held is that high-symmetry materials are usually good for thermoelectrics, leading to great efforts having historically been focused on GeTe alloys in a high-symmetry cubic structure. Here we show a slight reduction of crystal structure symmetry of GeTe alloys from cubic to rhombohedral, enabling a rearrangement in electronic bands for more transporting channels of charge carriers and many imperfections for more blocking centers of heat-energy carriers (phonons). This leads to the discovery of rhombohedral GeTe alloys as the most efficient thermoelectric materials to date, opening new possibilities for low-symmetry thermoelectric materials.

higher-symmetry pseudo-cubic has proved to be effective for improving thermoelectric performance.[17]

On the other hand, lower-symmetry materials have their advancements as thermoelectrics based upon inherently low lattice thermal conductivities (~1 W/m-K or less). These are typified by new materials such as SnSe,[18,19] Zn_4Sb_3,[20] CdSb,[21] MgAgSb,[22] $Yb_{14}MnSb_{11}$,[23] $Ca_9Zn_4Sb_9$,[24] and Mg_3Sb_2[25,26] and its ternary derivatives.[27] This is believed to be fundamentally due to structure complexity in these materials.[28–30] In addition, enhancement of phonon scattering to reduce lattice thermal conductivity has been successful using various mechanisms including point defects,[5] dislocations,[15,31,32] and nanostructures[33] in both cubic and non-cubic thermoelectrics.

The above principles suggest that it would be ideal if a thermoelectric could behave electronically as a high-symmetry material but thermally as a low-symmetry material. If the symmetry breaking of band degeneracy is small, both effects may be simultaneously realized, which suggests a strategy of symmetry optimization for making high-performance thermoelectrics.

Among known thermoelectrics, p-type IV-VI semiconductors have led most of the advancements and demonstrate the best performance above room temperature. Most thermoelectric IV-VI compounds crystallize in a cubic structure, and the high zT achieved is well known to be electronically due to the convergence of the L and low-lying Σ bands at high temperatures.[2] In addition to chemical substitution for reducing the energy offset of the L band relative to the Σ band,[2,34] this convergence can also originate from a change in the structure such as thermal expansion.[35]

These two bands have different symmetries from different locations within the Brillouin zone, and thus will be differently affected by different crystal lattice distortions. Directional lattice distortions, for example, might allow for explicit manipulation of the energy of a given band. Here we have found that a rhombohedral distortion along the [111] crystallographic direction (exact the L point of the Brillouin zone) in GeTe gradually reduces the energy of the L band relative to the Σ band so that the Σ band is the highest energy valence band in GeTe (Figure 1). Manipulating the degree of the rhombohedral distortion, which is called a symmetry reduction or a symmetry breaking in this work, can lead to band convergence of L and Σ bands.

This symmetry reduction also splits the 4 L pockets into 3 L + 1 Z and also 12 Σ pockets into 6 Σ + 6 η, making it seemingly more difficult to achieve band convergence. Nevertheless, the added degree of freedom to slowly tune the band energies is sufficient to achieve effective convergence of all the bands. Such manipulation of the band structure through crystal structure engineering creates the possibility that a slightly lower-symmetry material may electronically behave as well as or even better than the cubic analogs.

Among IV-VI compounds, GeTe is the only one having a stable rhombohedral structure at room temperature. Above 720 K,[37] GeTe transitions to a cubic structure typical of IV-VI compounds. Stemming from the very similar band structure in cubic GeTe as those of other high zT cubic IV-VI analogs, such as PbTe, PbSe, and SnTe, most of the existing literature (since the 1960s) on GeTe have focused on the high-temperature cubic phase and all the reported peak zT are enabled so far in the cubic phase only.

[1]Interdisciplinary Materials Research Center, School of Materials Science and Engineering, Tongji University, Shanghai 201804, China

[2]Department of Mechanical Engineering, The University of Hong Kong, Pokfulam Road, Hong Kong SAR, China

[3]State Key Laboratory of High Performance Ceramics and Superfine Microstructure, Shanghai Institute of Ceramics, CAS, Shanghai 200050, China

[4]Materials Science and Engineering, Northwestern University, Evanston, IL 60208, USA

[5]Lawrence Berkeley National Lab, 1 Cyclotron Road, Berkeley, CA, USA

[6]These authors contributed equally

[7]Lead Contact

*Correspondence: yanzhong@tongji.edu.cn

https://doi.org/10.1016/j.joule.2018.02.016

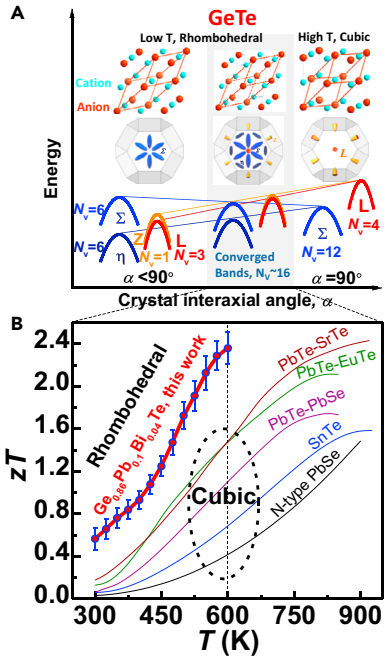

Figure 1. Symmetry Reduction for Enhancing Thermoelectric GeTe

(A and B) Evolution of crystal structure-dependent Fermi surface of the dominant transporting valence band(s) of GeTe (A), and zT with SD of measurements for rhombohedral GeTe, with a comparison with best-performance cubic IV-VI thermoelectrics (B).[2,6,31,32,36]

In this work, increasing the rhombohedral angle (a measure of the degree of directional lattice distortion along [111]), particularly through doping with Bi, creates a more favorable band structure for electronic performance (Figure 1A, shaded region). Combining the advantage of good electronic performance with a lower inherent lattice thermal conductivity[38] and additional phonon scattering by substitutional defects (both Pb alloying and Bi doping), this work realizes in rhombohedral GeTe a peak zT as high as ~2.4 at 600 K (Figure 1B), which is much higher than that of any of its cubic analogs.[2,6,31,32,36] Such a record zT stems from a slight symmetry reduction from a cubic structure, which simultaneously enables the rearrangement of split valence bands and the reduction in κ_L. This is significantly different from existing concepts for advancing thermoelectrics. Moreover, rhombohedral GeTe alloy has a zT higher than that of known high-performance thermoelectrics within 450–600 K and even shows a zT comparable with that of existing near-room-temperature (300–450 K) thermoelectric materials (Figure 2A). The device ZT[39] is found to be as high as 1.3 within 300–600 K (Figure 2B) and 1.5 in the entire working temperature range (Figure S1), being a record among all known thermoelectrics in any types of conduction.

RESULTS AND DISCUSSION

Detailed results on transport properties (Figure S2), carrier concentration (Figure S3), X-ray diffraction (XRD) (Figure S4), microstructure (Figure S5), and thermal stability (Figure S6) are provided in Supplemental Information. As shown in Figure S2, rhombohedral GeTe (r-GeTe) alloy shows a high weighted mobility and a greatly reduced lattice thermal conductivity as compared with pristine GeTe. These combined attributes give $Ge_{0.86}Pb_{0.1}Bi_{0.04}Te$ the highest quality factor (β) ensuring the highest possible electronic performance and figure of merit[46] among these high-zT IV-VI thermoelectrics.

The electrical performance of the r-GeTe alloy is comparable with the best, optimally band-converged PbTe (or any p-type IV-VI). Achieving electronic performance in

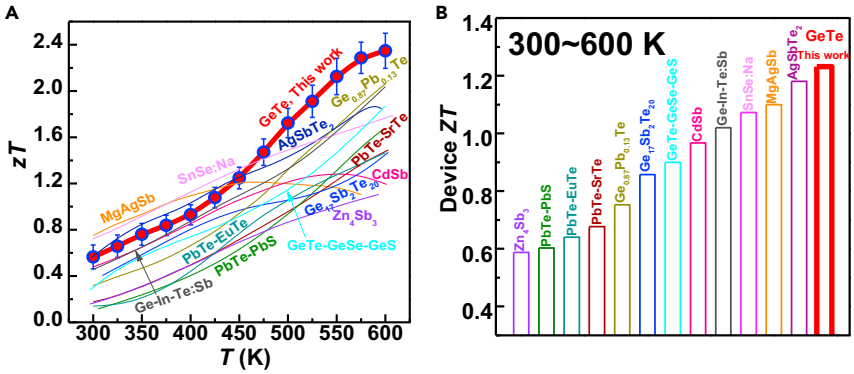

Figure 2. Thermoelectric Performance

(A and B) Comparison on thermoelectric figure of merit, zT (A) among known high-performance thermoelectrics[19–22,32,36,40–45] within 300–600 K, and their corresponding device ZT[39] (B).

r-GeTe equivalent to PbTe is remarkable because the reduced symmetry is expected to result in a comparatively lower density of states mass (m^*_{DOS}) and weighted mobility. This is observed in pristine r-GeTe without alloying, where a substantially lower m^*_{DOS} stemming from a lower degeneracy (N_v) creates a lower weighted mobility (Figure S2). However, when r-GeTe is nearly cubic as in the Pb- and Bi-doped alloys, the effective valley degeneracy is comparable with or even higher than that of PbTe. As a result, the single parabolic band (SPB) model determined m^*_{DOS} is slightly higher in r-GeTe than band-converged PbTe. This allows r-GeTe alloy to have a weighted mobility comparable with that of band-converged PbTe despite having a smaller overall carrier mobility. Pristine GeTe has slightly lighter conductivity masses (inertial mass) of the Σ band, enabling slightly higher mobility.[38] The r-GeTe alloyed with Pb and Bi has an inertial mass almost identical to that of pristine GeTe but a lower carrier mobility (Figure S2). This is due to a reduced relaxation time in the alloy, perhaps due to alloy scattering.

Calculated band structures taking the spin orbital coupling (SOC) effect into account for rhombohedral and cubic GeTe are shown in Figure 3. The results for r-GeTe are generally consistent with an earlier study[47] but also plot data along the sigma direction. Band structures of r-GeTe with and without SOC are compared in Figure S7. The L band in the cubic system lies along the [111] direction, and a lattice distortion along this direction yields a rhombohedral structure with a slightly reduced symmetry (Figure 1A). This results in several key differences between the rhombohedral and cubic systems in GeTe. First, the distortion results in a reduction in energy of the L and Z bands as compared with the L valence band in the cubic structure.[38] The reduction is significant enough to switch the valence band maximum from the L-type to the Σ-type bands as well as a significantly increase the band gap at L. Secondly, the four L pockets of the cubic system are split into three L and one Z pocket (with a very small energy offset and thus approximated as L-type bands in the following discussion) of the rhombohedral structure, and similarly the 12 Σ pockets become 6 Σ and 6 η. With the help of the spin-orbit interaction, the Z pocket of the rhombohedral structure moves slightly off Z and quickly becomes a ring that merges with Σ that may add more Fermi surface complexity.[48] As the distortion lessens with doping and temperature, the pocket moves back to Z. The reduction in energy offset between L-type and Σ bands ($\Delta E_{\Sigma-L}$) is found to be mainly due to the increase of interaxial angle (γ for primitive and α for unit cell; Figures 3E, S7, and S8). When taking both effects of atomic off-center displacements and lattice parameter change, L valence band is found to be

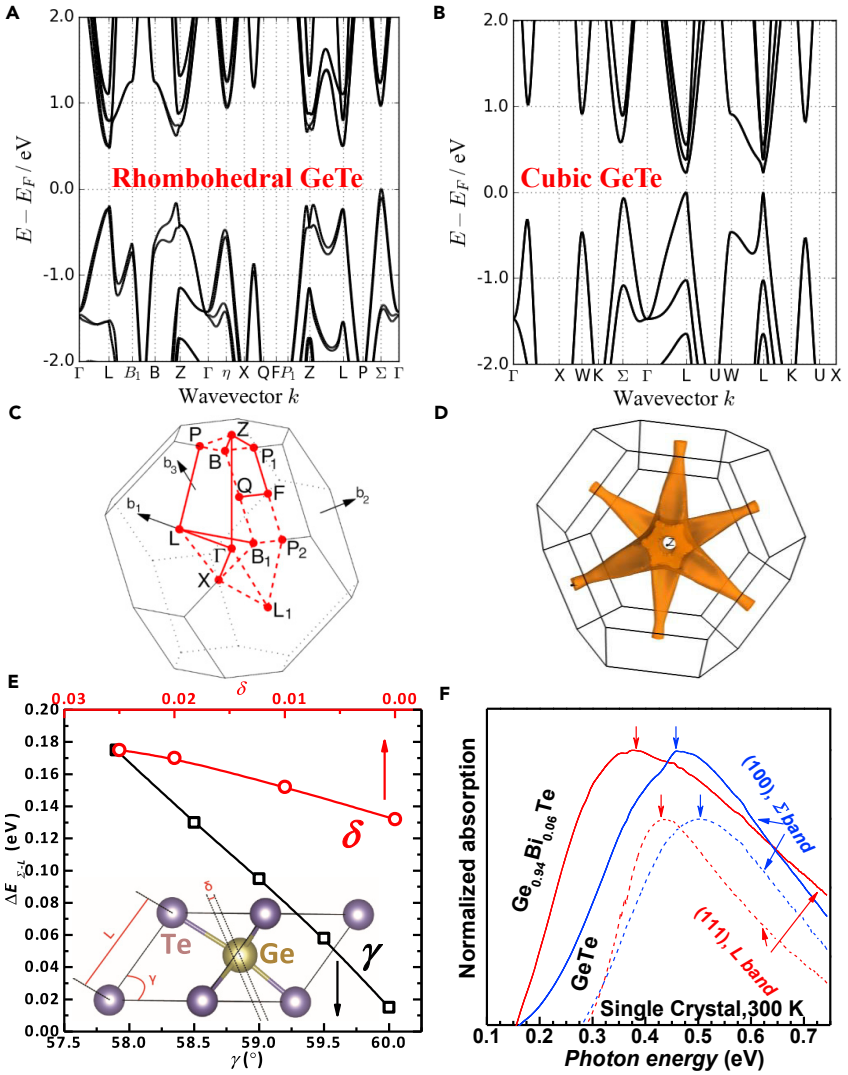

Figure 3. Band Structure

(A–F) Calculated band structure for rhombohedral (A) and cubic (B) GeTe with SOC; the Brillouin zone (C) and the Fermi surface (D) at 0.22 eV below the valance band maxima of rhombohedral GeTe; calculated interaxial angle (γ) and atomic off-center displacement (δ) dependent band offset ($\Delta E_{\Sigma-L}$) between *L* and Σ (E) for GeTe primitive cell (rhombohedral: $\gamma < 60°$; cubic: $\gamma = 60°$); and normalized infrared absorption versus photon energy at room temperature for single-crystal (F) $Ge_{0.9-y}Pb_{0.1}Bi_yTe$.

above that of Σ in the cubic structure (Figure 3). The band structure of doped GeTe is shown in Figure S9.

High-temperature XRD results reveal that GeTe with and without substitution both show a continuous increase in α toward 90° as the temperature increases (Figure S4). As this occurs, the three *L*-type (*L*) band pockets of the rhombohedral system converge with the Z to make the four *L* pockets of the cubic structure that becomes the valence band maximum. Doping with Bi is found to be particularly effective for increasing the low temperature interaxial angle (Figure S4) and thus reduces the temperature at which α reaches 90° (Figure S4). This decreases the temperature at which the bands are effectively converged when α is close to but slightly smaller

than 90°, for a higher weighted mobility in the alloy, as compared with the pristine GeTe (Figure S2). This change in the temperature dependence of the transport demonstrates crystal structure engineering as another degree of freedom for manipulating the band structure.

Plasma frequency measurements were used to further characterize the band structure. Single crystals of GeTe and $Ge_{0.94}Bi_{0.06}Te$ (Figure S10), respectively having carrier concentrations of 1×10^{21} cm^{-3} and 9×10^{20} cm^{-3}, ensure a distribution of carriers in both *L*-type and Σ-type bands. Measurements were performed along the [111] and [100] directions, respectively corresponding to the main axes of the *L*-type and Σ-type ellipsoidal Fermi surfaces. Using the Lyden approximation[49] (Table S1), it was found that the *L*-type band is ~0.08 eV lower in energy than that of the Σ-type band in GeTe and ~0.05 eV in $Ge_{0.94}Bi_{0.06}Te$. This experimentally confirms that the valence band maximum is located along the Σ direction in rhombohedral GeTe. Similar estimation of the Fermi energy for each band in single-crystal SnTe with a hole concentration of 5.6×10^{20} cm^{-3} reveals that *L* is above Σ by ~0.17 eV (Figure S11), in good agreement with band calculations.[38]

Measurements of polycrystalline materials with low carrier concentrations ($<5 \times 10^{20}$ cm^{-3}), as shown in Figure S12, enable an estimation of the mean inertial mass (m_I*)[49] of carriers as well (see Supplemental Information for more details). The obtained inertial mass is ~0.22 m_e for Σ valleys (Table S2), which is consistent with the band calculation[38] (~0.25 m_e) and much larger than that of the *L* band in PbTe (~0.13 m_e) or SnTe (~0.11 m_e). The band effective mass (m_b*) can then be estimated by $m_b^*1/3K^{1/3}(K^{-1} + 2)m_I^*$, where the band anisotropy factor $K = m_{||}^*/m_{\perp}^* = 6$ is taken. This further enables an estimation of the density of state effective mass (m_d*) via $m_d^* = N_v^{2/3}m_b^*$. This approximation results in an m_d^* of 1.1 m_e for the Σ band, which is consistent with density functional theory (DFT) calculations. The inertial effective mass of PbTe and SnTe are also included in Table S2, which are 30%–50% smaller than that of GeTe because of its principal valence band of Σ. It should be noted that GeTe single crystals in this work show carrier concentration-dependent Seebeck coefficient and mobility similar to those of polycrystals (Figure S13).

Figure 4 shows the temperature-dependent thermoelectric transport properties for the high *zT* compositions (heat capacity given in Figure S14), while those for all compositions are given in Figure S15. It is seen that the high thermoelectric performance is highly reproducible, which is ensured by multiple measurements and by different measurement apparatus on the same sample, as well as measurements on repeated samples with similar compositions. Similar reproducibility is also obtained in the entire working temperature as shown in Figure S16, enabling a reliable estimation of device $ZT = 1.5$. Moreover, the thermoelectric properties are found to be effectively isotropic in these polycrystalline materials (Figure S17).

Much of the high *zT* realized in r-GeTe alloys in this work is attributable to the low lattice thermal conductivity, which is largely due to its reduced symmetry and the additional phonon scattering by point defects (Pb and Bi substitutions). The lattice thermal conductivity is determined by subtracting the electronic contribution ($\kappa_e = LT/\rho$) from the total thermal conductivity, where the Lorenz factor, *L*, is estimated by a SPB model approximation with acoustic phonon scattering. Pure GeTe naturally has a carrier concentration as high as ~10^{21} cm^{-3} due to Ge vacancies and requires a high doping concentration and alloying (usually ≥10%) for compensation to achieve the optimum value (~1.5×10^{20} cm^{-3}). In this

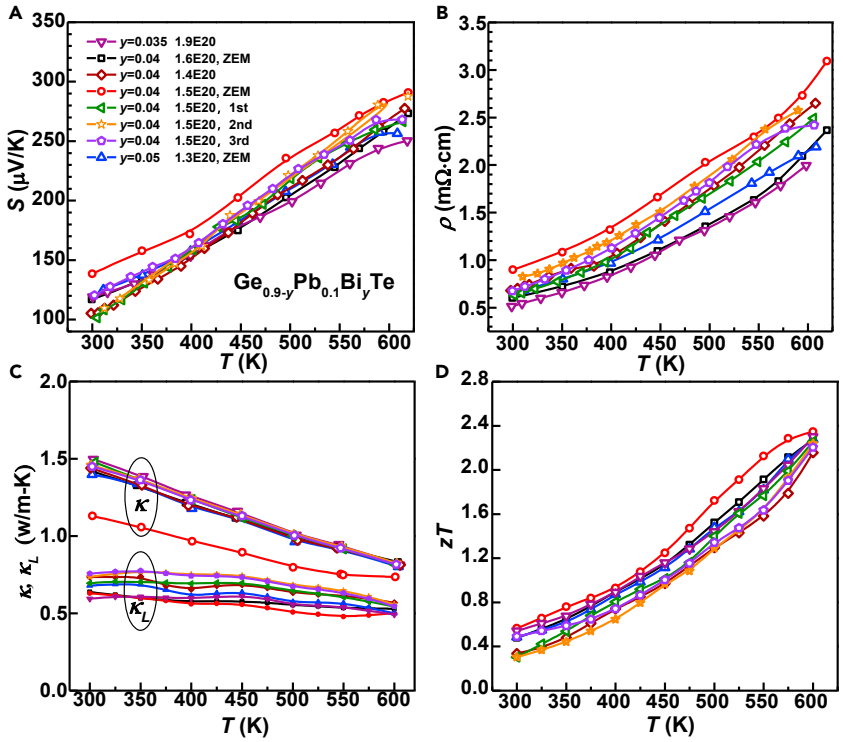

Figure 4. Transport Properties

(A–D) Temperature-dependent Seebeck coefficient (A), resistivity (B), thermal conductivity (C), and figure of merit (D) for $Ge_{0.9-y}Pb_{0.1}Bi_yTe$ alloys showing high zT.

work, both Pb and Bi ensure sufficient mass and size fluctuations for an effective reduction in lattice thermal conductivity from ~2.6 W/m-K in pristine GeTe to ~0.7 W/m-K in $Ge_{0.86}Pb_{0.1}Bi_{0.04}Te$ at room temperature (Figure 5A), which can be understood using the Debye-Callaway model (see Supplemental Information for more details). Moreover, additional thermal models based on full elastic tensor calculations by DFT confirm the reduction of thermal conductivity from cubic to rhombohedral (see Supplemental Information).

It should be noted that alloying may lead to a softening of optical modes for additional acoustic-optical interaction[50] and thus a reduction in lattice thermal conductivity (κ_L), which is not included in the thermal modeling. This effect simultaneously induces a reduction in sound velocity, which is confirmed by our measurements (Figure 5B) and has been accounted for in the modeling. Importantly, it is seen that the observed κ_L reduction mainly originates from point defect scattering, as concluded in the literature.[50]

To enhance zT through a symmetry reduction in general, the start high-symmetry material should have multiple bands but with energy offsets, and each band should have a high valley degeneracy due to symmetry. Depending on the degree of reduction in crystal structure symmetry, the original bands can be split in different ways to have different valley degeneracies, and the energy for these split bands can change very differently. These would all contribute to a rearrangement in energy of these split bands having various valley degeneracies for an enhanced electronic performance, if many split bands converge effectively to have a total valley degeneracy higher than that of the start high-symmetry material (Figure S18). In addition, symmetry reduction generally leads to a reduction in κ_L. For instance,

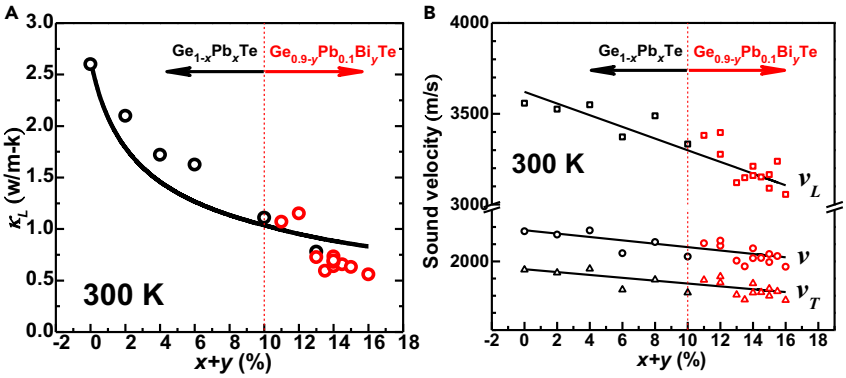

Figure 5. Thermal Conductivity and Sound Velocity

(A and B) Composition-dependent lattice thermal conductivity (A) and sound velocity (B) with a comparison with model prediction for $Ge_{1-x-y}Pb_xBi_yTe$ alloys.

cubic IV-VI and II_2-IV thermoelectrics, sharing the commonness of a two-band structure (with a band offset) whereby each band has a high valley degeneracy, enable many possibilities for enhancing the electronic performance as well as for reducing κ_L through control of symmetry breaking. Providing the above criteria are satisfied, low-symmetry materials would in principle show promising thermoelectric performance as well.

This work demonstrates that using a slight symmetry reduction of high-symmetry thermoelectrics, the high valley degeneracy can be ensured and combined with the low thermal conductivity due to complex structures. Distortion of the cubic lattice along the [111] direction leads to the desired heavier Σ valence bands higher in energy so that they dominate the electronic transport. Including compositional complexity by alloying with Pb and doping with Bi tunes the distortion and simultaneously enhances phonon scattering. As a result, both a record peak zT at 600 K and a record device ZT over the entire working temperature range are achieved in rhombohedral GeTe. This work not only promotes GeTe alloys as principal materials for thermoelectric power generation below 800 K, but also expands low-symmetry materials as efficient thermoelectrics.

EXPERIMENTAL PROCEDURES

Polycrystalline $Ge_{1-x}Pb_xTe$ ($x \leq 0.15$) and $Ge_{0.9-y}Pb_{0.1}Bi_yTe$ ($y \leq 0.06$) were synthesized by melting stoichiometric amounts of high-purity elements (>99.99%) under vacuum in quartz ampoules at 1,123 K for 6 hr, quenching in cold water, and annealing at 973 K for 3 days. The ingots were hand ground into fine powders for XRD and optical reflectance measurements by Fourier transform infrared spectroscopy (FTIR; Bruker Tensor 2 equipped with Diffuse Reflectance attachment) at room temperature. Temperature-dependent powder XRD was carried for samples GeTe and $Ge_{0.86}Pb_{0.1}Bi_{0.04}Te$ (Bruker, D8Advance). GeTe and $Ge_{0.94}Bi_{0.06}Te$ single crystals were grown by both Bridgman and zone melting methods, with a crucible lowing rate of 1–1.5 μm/s and a temperature of ~1,073 K for melting. Cleavage planes of {111} and {100} were used for XRD and FTIR measurements. The microstructure was characterized by a scanning electron microscope (Phenon-pro) equipped with energy-dispersive spectroscopy. Hot pressing was carried out by induction heating[51] at 873 K for 40 min under a uniaxial pressure of ~80 MPa. The obtained dense pellets (>98% of the theoretical density) were ~12 mm in diameter and ~1.5 mm in thickness for transport property measurements.

Resistivity, Seebeck coefficient, and Hall coefficient were simultaneously measured on the pellet samples, where the hot and cold side temperatures were measured by two K-type thermocouples attached to the opposite edges of the pellet sample and the thermopower was measured by two Nb wires welded to the thermocouple tips. Resistivity and Hall coefficients were measured using the Van der Pauw technique under a reversible magnetic field of 1.5 T. The Seebeck coefficient was obtained from the slope of the thermopower versus temperature difference from 0 to 5 K.[52] As a comparison, an Ulvac ZEM-3 apparatus was also used for Seebeck coefficient and resistivity measurements on high thermoelectric performance samples. The thermal diffusivity (D) was measured by a laser flash technique with the Netzsch LFA457 system. A differential scanning calorimetry (DSC) apparatus (DSC 404F3, Netzsch) was used to measure the heat capacity (Cp) and to check the stability of the samples. A Dulong-Petit limit of Cp is used, which is close to the average value of available literature results[53–56] and measurements in this work under different heating rates at temperatures not close to that of phase transition (Figure S14). In addition, most of the literature reporting a high zT in GeTe uses a heat capacity at or very close to the Dulong-Petit limit.[40–42,57–60] To have a consistent comparison on thermal conductivity and zT of high-performance GeTe thermoelectrics (Figures 2 and S1), it is therefore meaningful to show the transport property with a heat capacity of Dulong-Petit limit as well in this work. The thermal conductivity is determined via $\kappa = dCpD$, where d is the density determined by mass/volume. All transport property measurements were carried out from 300 to 800 K. Measurements of sound velocities were performed on pellet samples at room temperature. Longitudinal and transverse sound velocities were determined using a pulse-receiver (Olympus-NDT) equipped with an oscilloscope (Keysight). Couplant was applied between the sample and the ultrasonic transducers.

DFT calculations were carried out using the projector augmented wave method as implemented in VASP (Vienna *ab initio* simulation package).[61,62] The parameterization by Perdew, Burke, and Ernzerfhof[63] based on the generalized gradient approximation was applied to calculate the band structures. A 2 × 2 × 1 supercell containing 24 atoms was constructed with its Brillouin zone sampled with a 5 × 5 × 3 k-point mesh. The doped systems were obtained by substituting one Ge atom with one impurity atom (Bi or Pb), corresponding to a doping concentration of approximately 8.3%. The plane wave cutoff energy was set to 300 eV and atomic coordinates were relaxed until the total energy converged to 10^{-5} eV. The band-unfolding technique proposed by Medeiros et al.[64,65] was used to recover the effective band structures of doped GeTe from supercell calculations. The SOC effect was taken into account for band calculations for GeTe unit cell in both rhombohedral and cubic structures. For SOC calculations, the plane wave cutoff energy was set to 520 eV and a k-point mesh of 7 × 7 × 7 was used. We initialized SOC calculations with magnetic moment of 0.6 along the z axis in VASP. When comparing the band structures with and without SOC effects, we use the same settings (e.g., cutoff energy) for both calculations to make a better comparison. To plot the band structure and Fermi surfaces, we used the plotting tools available in the pymatgen[66] package.

XRD was used to characterize the phase in the obtained $Ge_{1-x}Pb_xTe$ ($x \leq 0.15$) and $Ge_{0.9-y}Pb0.1Bi_yTe$ ($y \leq 0.06$) alloys. Both alloying and doping lead to a continuous linear decrease in the Hall carrier concentration of 1–8 × 10^{20} cm^{-3} as shown in Figure S3 and Table S2. The further decrease in hole concentration due to Bi doping suggests the occupation of Bi on the Ge site, since the Bi/Te anti-site defect would behave as an acceptor and increase the hole concentration. All room temperature diffraction peaks can be well indexed to the rhombohedral structure of GeTe with a unit cell shown in Figure 1A, when $x \leq 0.1$ and $y \leq 0.06$. It is seen that Pb- and Bi-substitution respectively increases the lattice parameter and the interaxial angle (Figure S4). An impurity phase of PbTe

at $x = 0.15$ was observed by a scanning electron microscope in literature,[60,67–70] while the rest of the $Ge_{1-x}Pb_xTe$ materials synthesized in this work were found to be single phase with a homogeneous distribution of constituent elements (Figure S5). Trace of Ge can be observed, which is typical of GeTe. Pb- and Bi-substitution lead to a lower temperature that stabilizes the lattice as cubic (Figure S4), which is consistent with the DSC measurements (Figure S6). All the materials here show a phase transition at temperatures above 600 K (Figure S6). Therefore, this work focuses on the thermoelectric transport properties within 300–600 K.

SUPPLEMENTAL INFORMATION

Supplemental Information includes Supplemental Experimental Procedures, 18 figures, and 5 tables and can be found with this article online at https://doi.org/10.1016/j.joule.2018.02.016.

ACKNOWLEDGMENTS

This work is supported by the National Natural Science Foundation of China (grant no. 11474219 and 51772215) and the National Recruitment Program of Global Youth Experts (1000 Plan). Y.C. acknowledges financial support from the Early Career Scheme of RGC under Project Number 27202516 and the research computing facilities offered by ITS, HKU. G.J.S. and I.T.W. acknowledge funding from the Solid-State Solar-Thermal Energy Conversion Center (S3TEC), an Energy Frontier Research Center, funded by the US Department of Energy, Office of Science, Basic Energy Sciences (DE-SC0001299). A.J. and A.F. acknowledge support from the US Department of Energy, Office of Basic Energy Sciences, Early Career Research Program (ECRP). Computing resources were provided by the National Energy Research Scientific Computing Center (NERSC), a DOE Office of Science User Facility supported by the Office of Science of the US Department of Energy under contract no. DE-AC02-05CH11231.

AUTHOR CONTRIBUTIONS

Conceptualization, Y.P.; Experiments, J.L. and X.Z. (equal contribution); DFT calculations, J.S., A.F., A.J., and Y.C.; Discussion, Y.P., G.J.S., and L.C.; Writing and Revision, J.L., X.Z., Z.C., S.L., W.L., J.S., I.T.W., A.F., Y.C., A.J., L.C., G.J.S., and Y.P.

DECLARATION OF INTERESTS

The authors declare no competing interests.

Received: January 29, 2018
Revised: February 12, 2018
Accepted: February 20, 2018
Published: March 9, 2018

REFERENCES

1. Bell, L.E. (2008). Cooling, heating, generating power, and recovering waste heat with thermoelectric systems. Science *321*, 1457–1461.

2. Pei, Y., Shi, X., LaLonde, A., Wang, H., Chen, L., and Snyder, G.J. (2011). Convergence of electronic bands for high performance bulk thermoelectrics. Nature *473*, 66–69.

3. DiSalvo, F.J. (1999). Thermoelectric cooling and power generation. Science *285*, 703–706.

4. Lin, S., Li, W., Chen, Z., Shen, J., Ge, B., and Pei, Y. (2016). Tellurium as a high-performance elemental thermoelectric. Nat. Commun. *7*, 10287.

5. Vining, C.B. (1995). Silicon germanium. In CRC Handbook of Thermoelectrics, D.M. Rowe, ed. (CRC Press), pp. 329–337.

6. Li, W., Zheng, L., Ge, B., Lin, S., Zhang, X., Chen, Z., Chang, Y., and Pei, Y. (2017). Promoting SnTe as an eco-friendly solution for p-PbTe thermoelectric via band convergence and interstitial defects. Adv. Mater. *29*, https://doi.org/10.1002/adma.201605887.

7. Li, W., Chen, Z., Lin, S., Chang, Y., Ge, B., Chen, Y., and Pei, Y. (2015). Band and scattering tuning for high performance thermoelectric $Sn_{1-x}Mn_xTe$ alloys. J. Materiomics *1*, 307–315.

8. Liu, W., Tan, X., Yin, K., Liu, H., Tang, X., Shi, J., Zhang, Q., and Uher, C. (2012). Convergence of conduction bands as a means of enhancing thermoelectric performance of n-type

$Mg_2Si_{1-x}Sn_x$ solid solutions. Phys. Rev. Lett. *108*, 166601.

9. Tang, Y., Gibbs, Z.M., Agapito, L.A., Li, G., Kim, H.-S., Nardelli, M.B., Curtarolo, S., and Snyder, G.J. (2015). Convergence of multi-valley bands as the electronic origin of high thermoelectric performance in $CoSb_3$ skutterudites. Nat. Mater. *14*, 1223–1228.

10. Tyagi, K., Gahtori, B., Bathula, S., Auluck, S., and Dhar, A. (2014). Band structure and transport studies of copper selenide: an efficient thermoelectric material. Appl. Phys. Lett. *105*, 173905.

11. Barabash, S.V., and Ozolins, V. (2010). Order, miscibility, and electronic structure of Ag(Bi,Sb)Te2alloys and (Ag,Bi,Sb)Te precipitates in rocksalt matrix: a first-principles study. Phys. Rev. B *81*, 075212.

12. May, A.F., Flage-Larsen, E., and Snyder, G.J. (2010). Electron and phonon scattering in the high-temperature thermoelectric $La_3Te_{4-z}M_z$ (M= Sb, Bi). Phys. Rev. B *81*, 125205.

13. Wunderlich, W., Amano, M., and Matsumura, Y. (2014). Electronic band-structure calculations of $Ba_8Me_xSi_{46-x}$ clathrates with Me= Mg, Pd, Ni, Au, Ag, Cu, Zn, Al, Sn. J. Electron. Mater. *43*, 1527–1532.

14. Fu, C., Bai, S., Liu, Y., Tang, Y., Chen, L., Zhao, X., and Zhu, T. (2015). Realizing high figure of merit in heavy-band p-type half-Heusler thermoelectric materials. Nat. Commun. *6*, 8144.

15. Kim, S.I., Lee, K.H., Mun, H.A., Kim, H.S., Hwang, S.W., Roh, J.W., Yang, D.J., Shin, W.H., Li, X.S., Lee, Y.H., et al. (2015). Dense dislocation arrays embedded in grain boundaries for high-performance bulk thermoelectrics. Science *348*, 109–114.

16. Kim, H.-S., Heinz, N.A., Gibbs, Z.M., Tang, Y., Kang, S.D., and Snyder, G.J. (2017). High thermoelectric performance in $(Bi_{0.25}Sb_{0.75})_2Te_3$ due to band convergence and improved by Carrier concentration control. Mater. Today *20*, 452–459.

17. Zhang, J., Liu, R., Cheng, N., Zhang, Y., Yang, J., Uher, C., Shi, X., Chen, L., and Zhang, W. (2014). High-performance pseudocubic thermoelectric materials from non-cubic chalcopyrite compounds. Adv. Mater. *26*, 3848–3853.

18. Zhao, L.-D., Lo, S.-H., Zhang, Y., Sun, H., Tan, G., Uher, C., Wolverton, C., Dravid, V.P., and Kanatzidis, M.G. (2014). Ultralow thermal conductivity and high thermoelectric figure of merit in SnSe crystals. Nature *508*, 373–377.

19. Zhao, L.D., Tan, G., Hao, S., He, J., Pei, Y., Chi, H., Wang, H., Gong, S., Xu, H., Dravid, V.P., et al. (2015). Ultrahigh power factor and thermoelectric performance in hole-doped single-crystal SnSe. Science *10*, 1–7.

20. Snyder, G.J., Christensen, M., Nishibori, E., Caillat, T., and Iversen, B.B. (2004). Disordered zinc in Zn_4Sb_3 with phonon-glass and electron-crystal thermoelectric properties. Nat. Mater. *3*, 458–463.

21. Wang, S., Yang, J., Wu, L., Wei, P., Yang, J., Zhang, W., and Grin, Y. (2015). Anisotropic multicenter bonding and high thermoelectric performance in electron-poor CdSb. Chem. Mater. *27*, 1071–1081.

22. Zhao, H., Sui, J., Tang, Z., Lan, Y., Jie, Q., Kraemer, D., McEnaney, K., Guloy, A., Chen, G., and Ren, Z. (2014). High thermoelectric performance of MgAgSb-based materials. Nano Energy *7*, 97–103.

23. Brown, S.R., Kauzlarich, S.M., Gascoin, F., and Snyder, G.J. (2006). $Yb_{14}MnSb_{11}$: new high efficiency thermoelectric material for power generation. Chem. Mater. *18*, 1873–1877.

24. Wu, Z., Li, J., Li, X., Zhu, M., Wu, K.-c., Tao, X.-t., Huang, B.-B., and Xia, S.-q. (2016). Tuning the thermoelectric properties of $Ca_9Zn_{4+x}Sb_9$ by controlled doping on the interstitial structure. Chem. Mater. *28*, 6917–6924.

25. Zhang, J., Song, L., Pedersen, S.H., Yin, H., Hung, L.T., and Iversen, B.B. (2017). Discovery of high-performance low-cost n-type Mg_3Sb_2-based thermoelectric materials with multi-valley conduction bands. Nat. Commun. *8*, 13901.

26. Ohno, S., Imasato, K., Anand, S., Tamaki, H., Kang, S.D., Gorai, P., Sato, H.K., Toberer, E.S., Kanno, T., and Snyder, G.J. (2017). Phase boundary mapping to obtain n-type Mg_3Sb_2-based thermoelectrics. Joule *2*, 141–154.

27. Zhang, J., Song, L., Madsen, G.K., Fischer, K.F., Zhang, W., Shi, X., and Iversen, B.B. (2016). Designing high-performance layered thermoelectric materials through orbital engineering. Nat. Commun. *7*, 10892.

28. Snyder, G.J., and Toberer, E.S. (2008). Complex thermoelectric materials. Nat. Mater. *7*, 105–114.

29. Lin, S., Li, W., Li, S., Zhang, X., Chen, Z., Xu, Y., Chen, Y., and Pei, Y. (2017). High thermoelectric performance of Ag_9GaSe_6 enabled by low cutoff frequency of acoustic phonons. Joule *1*, 1–15.

30. Li, W., Lin, S., Ge, B., Yang, J., Zhang, W., and Pei, Y. (2016). Low sound velocity contributing to the high thermoelectric performance of Ag_8SnSe_6. Adv. Sci. *3*, 1600196.

31. Chen, Z., Ge, B., Li, W., Lin, S., Shen, J., Chang, Y., Hanus, R., Snyder, G.J., and Pei, Y. (2017). Vacancy-induced dislocations within grains for high-performance PbSe thermoelectrics. Nat. Commun. *8*, 13828.

32. Chen, Z., Jian, Z., Li, W., Chang, Y., Ge, B., Hanus, R., Yang, J., Chen, Y., Huang, M., Snyder, G.J., et al. (2017). Lattice dislocations enhancing thermoelectric PbTe in addition to band convergence. Adv. Mater. *29*, https://doi.org/10.1002/adma.201606768.

33. Hsu, K.F., Loo, S., Guo, F., Chen, W., Dyck, J.S., Uher, C., Hogan, T., Polychroniadis, E.K., and Kanatzidis, M.G. (2004). Cubic $AgPb_mSbTe_{2+m}$: bulk thermoelectric materials with high figure of merit. Science *303*, 818–821.

34. Zeier, W.G., Zevalkink, A., Gibbs, Z.M., Hautier, G., Kanatzidis, M.G., and Snyder, G.J. (2016). Thinking like a chemist: intuition in thermoelectric materials. Angew. Chem. Int. Ed. *55*, 6826–6841.

35. Ravich, Y.I., Efimova, B.A., and Smirnov, I.A. (1970). Semiconducting Lead Chalcogenides (Plenum Press).

36. Tan, G., Shi, F., Hao, S., Zhao, L.-D., Chi, H., Zhang, X., Uher, C., Wolverton, C., Dravid, V.P., and Kanatzidis, M.G. (2016). Non-equilibrium processing leads to record high thermoelectric figure of merit in PbTe-SrTe. Nat. Commun. *7*, 12167.

37. Chattopadhyay, T., Boucherle, J.X., and vonSchnering, H.G. (1987). Neutron diffraction study on the structural phase transition in GeTe. J. Phys. C Solid State Phys. *20*, 1431–1440.

38. Li, J., Chen, Z., Zhang, X., Sun, Y., Yang, J., and Pei, Y. (2017). Electronic origin of the high thermoelectric performance of GeTe among the p-type group IV monotellurides. NPG Asia Mater. *9*, e353.

39. Snyder, G.J. (2006). Thermoelectric power generation: efficiency and compatibility. In Thermoelectrics Handbook: Macro to Nano, D.M. Rowe, ed. (CRC/Taylor & Francis), pp. 9.1–9.26.

40. Samanta, M., and Biswas, K. (2017). Low thermal conductivity and high thermoelectric performance in $(GeTe)_{1-2x}$ $(GeSe)_x$ $(GeS)_x$: competition between solid solution and phase separation. J. Am. Chem. Soc. *139*, 9382–9391.

41. Williams, J.B., and Morelli, D.T. (2016). Understanding the superior thermoelectric performance of Sb precipitated $Ge_{17}Sb_2Te_{20}$. J. Mater. Chem. C *4*, 10011–10017.

42. Gelbstein, Y., Davidow, J., Girard, S.N., Chung, D.Y., and Kanatzidis, M. (2013). Controlling metallurgical phase separation reactions of the $Ge_{0.87}Pb_{0.13}Te$ alloy for high thermoelectric performance. Adv. Energy Mater. *3*, 815–820.

43. Wu, D., Zhao, L.-D., Tong, X., Li, W., Wu, L., Tan, Q., Pei, Y., Huang, L., Li, J.-F., Zhu, Y., et al. (2015). Superior thermoelectric performance in PbTe-PbS pseudo-binary: extremely low thermal conductivity and modulated carrier concentration. Energy Environ. Sci. *8*, 2056–2068.

44. Hong, M., Chen, Z.G., Yang, L., Zou, Y.C., Dargusch, M.S., Wang, H., and Zou, J. (2018). Realizing zT of 2.3 in $Ge_{1-x-y}Sb_xIn_yTe$ via reducing the phase-transition temperature and introducing resonant energy doping. Adv. Mater. https://doi.org/10.1002/adma.201705942.

45. Roychowdhury, S., Panigrahi, R., Perumal, S., and Biswas, K. (2017). Ultrahigh thermoelectric figure of merit and enhanced mechanical stability of p-type $AgSb_{1-x}Zn_xTe_2$. ACS Energy Lett. *2*, 349–356.

46. Goldsmid, H.J. (2009). Introduction to Thermoelectricity (Springer).

47. Di Sante, D., Barone, P., Bertacco, R., and Picozzi, S. (2013). Electric control of the giant rashba effect in bulk GeTe. Adv. Mater. *25*, 509–513.

48. Gibbs, Z.M., Ricci, F., Li, G., Zhu, H., Persson, K., Ceder, G., Hautier, G., Jain, A., and Snyder, G.J. (2017). Effective mass and Fermi surface complexity factor from ab initio band structure calculations. NPJ Comput. Mater. *3*, 8.

49. Lyden, H.A. (1964). Measurement of the conductivity effective mass in semiconductors using infrared reflection. Phys. Rev. *134*, A1106–A1112.

50. Murphy, R.M., Murray, É.D., Fahy, S., and Savić, I. (2017). Ferroelectric phase transition and the lattice thermal conductivity of $Pb_{1-x}Ge_xTe$ alloys. Phys. Rev. B *95*, 144302.

51. LaLonde, A.D., Ikeda, T., and Snyder, G.J. (2011). Rapid consolidation of powdered materials by induction hot pressing. Rev. Sci. Instrum. *82*, 025104.

52. Zhou, Z.H., and Uher, C. (2005). Apparatus for Seebeck coefficient and electrical resistivity measurements of bulk thermoelectric materials at high temperature. Rev. Sci. Instrum. *76*, 023901.

53. Sun, H., Lu, X., Chi, H., Morelli, D.T., and Uher, C. (2014). Highly efficient $(In_2Te_3)x(GeTe)(3-3x)$ thermoelectric materials: a substitute for TAGS. Phys. Chem. Chem. Phys. *16*, 15570–15575.

54. Perumal, S., Bellare, P., Shenoy, U.S., Waghmare, U.V., and Biswas, K. (2017). Low thermal conductivity and high thermoelectric performance in Sb and Bi codoped GeTe: complementary effect of band convergence and nanostructuring. Chem. Mater. *29*, 10426–10435.

55. Yang, L., Li, J.Q., Chen, R., Li, Y., Liu, F.S., and Ao, W.Q. (2016). Influence of Se substitution in GeTe on phase and thermoelectric properties. J. Electron. Mater. *45*, 5533–5539.

56. Perumal, S., Roychowdhury, S., and Biswas, K. (2016). Reduction of thermal conductivity through nanostructuring enhances the thermoelectric figure of merit in $Ge_{1-x}Bi_xTe$. Inorg. Chem. Front. *3*, 125–132.

57. Welzmiller, S., Fahrnbauer, F., Hennersdorf, F., Dittmann, S., Liebau, M., Fraunhofer, C., Zeier, W.G., Snyder, G.J., and Oeckler, O. (2015). Increasing seebeck coefficients and thermoelectric performance of Sn/Sb/Te and Ge/Sb/Te materials by Cd doping. Adv. Electron. Mater. *1*, 1500266.

58. Fahrnbauer, F., Souchay, D., Wagner, G., and Oeckler, O. (2015). High thermoelectric figure of merit values of germanium antimony tellurides with kinetically stable cobalt germanide precipitates. J. Am. Chem. Soc. *137*, 12633–12638.

59. Wu, D., Zhao, L.D., Hao, S.Q., Jiang, Q.K., Zheng, F.S., Doak, J.W., Wu, H.J., Chi, H., Gelbstein, Y., Uher, C., et al. (2014). Origin of the high performance in GeTe-based thermoelectric materials upon Bi_2Te_3 doping. J. Am. Chem. Soc. *136*, 11412–11419.

60. Gelbstein, Y., and Davidow, J. (2014). Highly efficient functional $Ge_xPb_{1-x}Te$ based thermoelectric alloys. Phys. Chem. Chem. Phys. *16*, 20120–20126.

61. Kresse, G., and Furthmüller, J. (1996). Efficient iterative schemes for ab initio total-energy calculations using a plane-wave basis set. Phys. Rev. B *54*, 169–186.

62. Kresse, G., and Furthmüller, J. (1996). Efficiency of ab-initio total energy calculations for metals and semiconductors using a plane-wave basis set. Comput. Mater. Sci. *6*, 15–50.

63. Perdew, J.P., Burke, K., and Ernzerhof, M. (1996). Generalized gradient approximation made simple. Phys. Rev. Lett. *77*, 3865–3868.

64. Medeiros, P.V.C., Stafström, S., and Björk, J. (2014). Effects of extrinsic and intrinsic perturbations on the electronic structure of graphene: retaining an effective primitive cell band structure by band unfolding. Phys. Rev. B *89*, https://doi.org/10.1103/PhysRevB.89.041407.

65. Medeiros, P.V.C., Tsirkin, S.S., Stafström, S., and Björk, J. (2015). Unfolding spinor wave functions and expectation values of general operators: introducing the unfolding-density operator. Phys. Rev. B *91*, https://doi.org/10.1103/PhysRevB.91.041116.

66. Ong, S.P., Richards, W.D., Jain, A., Hautier, G., Kocher, M., Cholia, S., Gunter, D., Chevrier, V.L., Persson, K.A., and Ceder, G. (2013). Python Materials Genomics (pymatgen): a robust, open-source python library for materials analysis. Comput. Mater. Sci. *68*, 314–319.

67. Hazan, E., Madar, N., Parag, M., Casian, V., Ben-Yehuda, O., and Gelbstein, Y. (2015). Effective electronic mechanisms for optimizing the thermoelectric properties of GeTe-rich alloys. Adv. Electron. Mater. *1*, 1500228.

68. Hazan, E., Ben-Yehuda, O., Madar, N., and Gelbstein, Y. (2015). Functional graded germanium-lead chalcogenide-based thermoelectric module for renewable energy applications. Adv. Energy Mater. *5*, 1500272.

69. Gelbstein, Y. (2013). Phase morphology effects on the thermoelectric properties of $Pb_{0.25}Sn_{0.25}Ge_{0.5}Te$. Acta Mater. *61*, 1499–1507.

70. Dado, B., Gelbstein, Y., Mogilansky, D., Ezersky, V., and Dariel, M.P. (2009). Structural evolution following spinodal decomposition of the pseudoternary compound $(Pb_{0.3}Sn_{0.1}Ge_{0.6})Te$. J. Electron. Mater. *39*, 2165–2171.